Supplementary Information for

Buried interface defect regulation enables efficient and stable inverted perovskite solar cells

Zhichun Yang[a,b,*], Jiajing Wang[a,b], Jiaqi Ren[a,b], Chen Chen[a,b], Mengyu Li[a,b], Changgang Yang[a,b], Guofeng Zhang[a,b], Ruiyun Chen[a,b], Chengbing Qin[a,b], Liantuan Xiao[a,b], Suotang Jia[a,b], Waqar Ahmad[c,*]

[a] State Key Laboratory of Quantum Optics Technologies and Devices, Institute of Laser Spectroscopy, Shanxi University, Taiyuan 030006, China

[b] Collaborative Innovation Center of Extreme Optics, Shanxi University, Taiyuan 030006, China

[c] Department of Physics, Qilu Institute of Technology, Jinan 250200, China

*Corresponding authors

E-mail addresses: yangzhichun@sxu.edu.cn (Z. Yang), waqar.ahmad@qlit.edu.cn (W. Ahmad).

1. Experimental Section

1.1 Materials

Formamidinium iodide (FAI, 99.99%), lead (II) iodide (PbI_2, 99.999%), indium-doped tin oxide (ITO, 15 Ω sq^{-1}) glasses, and nickel oxide (NiO_x) nanoparticle were provided by Advanced Election Technology Co., Ltd. N, N-dimethylformamide (DMF, 99.8%), dimethyl sulfoxide (DMSO, 99.7%), isopropanol (IPA, 99.5%), ethyl acetate (EA, 99.5%), ethanol (99.99%), and chlorobenzene (CB, 99.8%) were purchased from J&K. 4-(3,6-Dimethoxy-9H-carbazol-9-yl)butyl)phosphonic acid (MeO-4PACz, 99%), Phenethylamine hydroiodide (PEAI, 99.5%), [6,6]-Phenyl-C61-butyric acid methyl ester (PCBM) and bathocuproine (BCP, 99.5%) were obtained from Xi'an Yuri Solar Co., Ltd., China. *p*-Fluorophenylacetic acid, *p*-Chlorophenylacetic acid, *p*-Bromophenylacetic acid, and *p*-Iodophenylacetic acid were purchased from Shanghai Macklin Biochemical Co., Ltd. Cesium bromide (CsBr, > 99.0%) was purchased from TCI. SnO_2 colloidal dispersion (15 wt% in H_2O) was purchased from Alfa Aesar. Aluminium oxide (Al_2O_3) nanoparticles (<50 nm, 20 wt.% in isopropanol) was purchased from Sigma Aldrich. Silver particles were provided by commercial sources.

1.2 Device fabrication

All devices were fabricated with an ITO/MeO-4PACz/ Al_2O_3/*p*-XPA (X = F, Cl, Br, I)/perovskite/PEAI/PCBM/BCP/Ag architecture and all steps were carried out in a nitrogen-filled glovebox. Indium tin oxide (ITO) glass substrates were first patterned using a nanosecond pulsed laser (wavelength: 355 nm, power: 3 W) to define the electrodes, followed by sequential ultrasonic cleaning in detergent, glass cleaner,

deionized water, ethanol, acetone, and isopropanol for 20 minutes, respectively. The cleaned substrates were then dried in an oven at 100 °C and treated with UV–ozone for 20 minutes prior to transfer into the glovebox. A self-assembled monolayer (SAM) of MeO-4PACz was deposited by spin-coating a 1 mg mL^{-1} ethanol solution at 6000 r.p.m. for 30 s, followed by annealing at 100 °C for 10 min. Then, it was spin-coated with an Al_2O_3 solution (1: 40 in IPA, volume ratio) at 6000 r.p.m. for 30 s, and annealed at 120 °C for 10 min. Subsequently, the *p*-XPA (X = F, Cl, Br, I) in isopropanol (IPA) at different concentrations were spin-coated onto the Al_2O_3 layer at 6000 r.p.m. for 30 s and annealed at 120 °C for 10 min to form the buried interface modification layer. The perovskite active layer with a composition of $Cs_{0.15}FA_{0.85}Pb(I_{0.95}Br_{0.15})_3$ was prepared from a 1.5 M precursor solution containing CsBr (0.0479 g), FAI (0.2193 g), and PbI_2 (0.6915 g) dissolved in 1 mL of DMF/DMSO (4:1 v/v) and stirred for 8 h. About 80 μL of the precursor solution was spin-coated onto the substrates at 5000 r.p.m. for 60 s with an acceleration of 3000 r.p.m. during which 300 μL of ethyl acetate was rapidly dripped at 15 s as antisolvent. The resulted films were annealed at 110 °C for 15 min to form perovskite layer. Then, PEAI solution at a concentration of 1 mg mL^{-1} in IPA was dynamically spin-coated onto the top at 6000 r.p.m. for 30 s and annealed at 110 °C for 10 min. For the electron transport layer, a 20 mg mL^{-1} PCBM solution in chlorobenzene was spin-coated at 3000 r.p.m. for 30 s and annealed at 70 °C for 10 min, followed by the deposition of a supersaturated bathocuproine (BCP) solution in IPA at 6000 r.p.m. for 30 s. Finally, a 100 nm Ag electrode was thermally evaporated through a shadow mask under high vacuum ($<5 \times 10^{-4}$ Pa) at a rate of 0.1–0.5 Å s^{-1} to

complete the device fabrication. The active area of each device was 0.09 cm^2.

2. Characterizations

The surface morphologies of perovskite films and cross-sectional view of the assembled devices were observed using Field-Emission scanning electron microscopy (SEM, Hitachi SU 8010, Japan). The roughness, morphological images, and Kelvin probe force microscopy (KPFM) measurements of perovskite films were acquired using Bruker Dimension Icon Atomic force microscopy (AFM) system. The crystal structures of perovskite films were determined using X-ray diffraction (XRD) equipped with a diffractometer employing Cu Kα radiation (D2 PHASER, Bruker). X-ray photoelectron spectroscopy (XPS) spectra were measured using a K-Alpha + spectrometer (K-Alpha, Thermo Scientific). Fourier transform infrared spectroscopy (FTIR) data was obtained using iS50 FT-IR (Nicolet). Ultraviolet photoelectron spectroscopy (UPS) was carried out by the Escalab Xi+ (Thermo Fisher). The absorption spectra of perovskite films were measured by an ultraviolet-visible (UV-vis) spectrophotometer (UNIC 3802, China). Steady-state photoluminescence (PL) was collected by an MS starter 100 Microscopic Spectroscopy system. Time-resolved PL (TRPL) spectra were recorded by a transient fluorescence spectrometer (Edinburgh instruments, FLS 980-STM, wavelength at 375 nm ± 10 nm). The electrochemical impedance spectroscopy (EIS) and Mott-Schottky measurements were performed by an Electrochemical Workstation (CHI 760E, China). The transient photovoltage (TPV) and current (TPC) decay measurements were carried out by a homemade transient photoelectric test system coupled with a Function Waveform Generator (SDG 1022X) and MSO24 Mixed signal

oscilloscope (Tektronix). Femtosecond transient absorption spectroscopy (fs-TAS) was carried out by the Ultrafast Transient Absorption Spectrometer (TIME-TECH SPECTRA). The dark current density and space charge limited current (SCLC) results were collected by a highly accurate source meter (2602B, Keithley) in dark conditions. The electrostatic potential (ESP) of DMPA was performed by Gaussian 09w software package. *J-V* curves of the fabricated solar cells were measured in ambient air by a Keithley 2400 source meter under simulated AM 1.5G (100 mW cm^{-2}) provided by a solar simulator (Beijing Zhongke Shicheng Technology Co., Ltd, SCX-100A, China). The light intensity was calibrated by a silicon reference cell (91150 V, Newport). The external quantum efficiency (EQE) was recorded by a photodetector measurement system (FineDet 900, China), which was equipped with a Xenon lamp, a monochromator, and a standard silicon detector for calibration. The operational stability of devices was carried out by a commercial multichannel stability test system (Wuhan 91PVKSolar). The light illumination was achieved by a 1 sun-equivalent white-light LED and the light intensity was calibrated to achieve the same J_{SC} from the devices measured under a standard solar simulator (AM 1.5 G, 100 mW cm^{-2}).

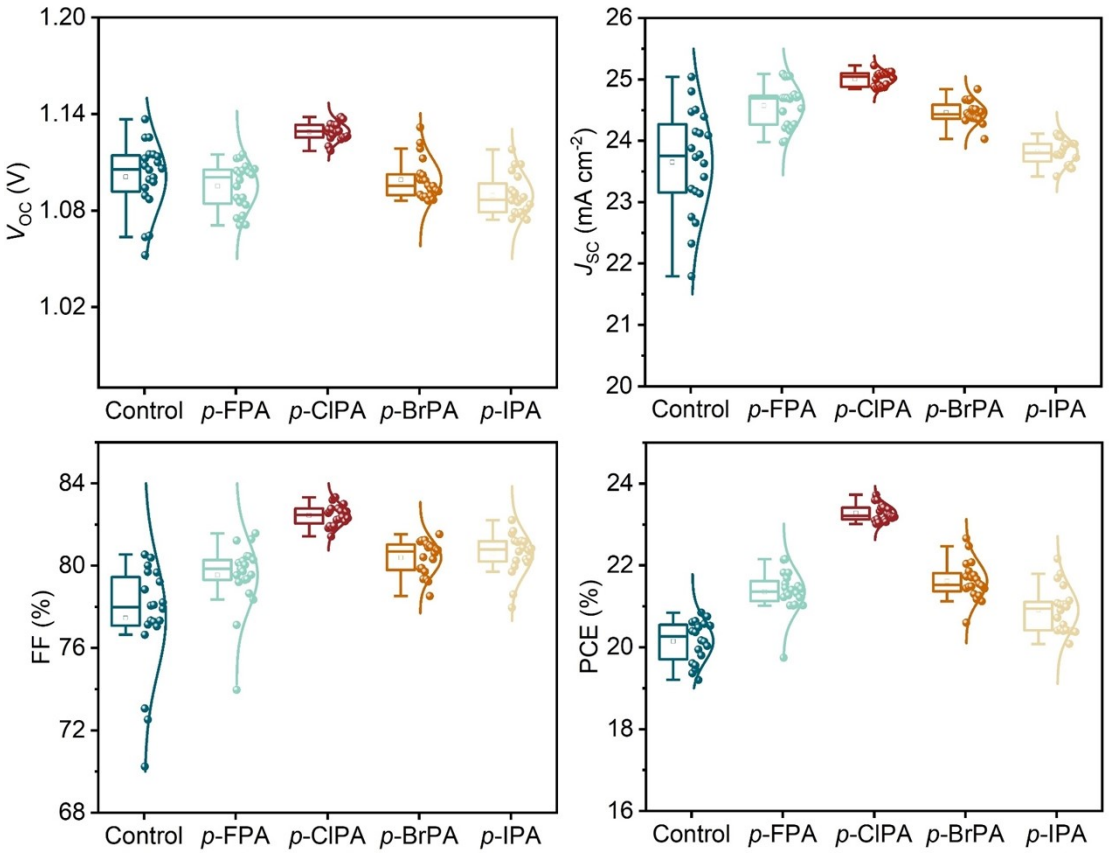

Fig. S1. Performance statistics of V_{OC}, J_{SC}, FF, and PCE for the control and *p*-XPA (X=F, Cl, Br, I)-modified devices at a concentration of 1 mg mL^{-1}.

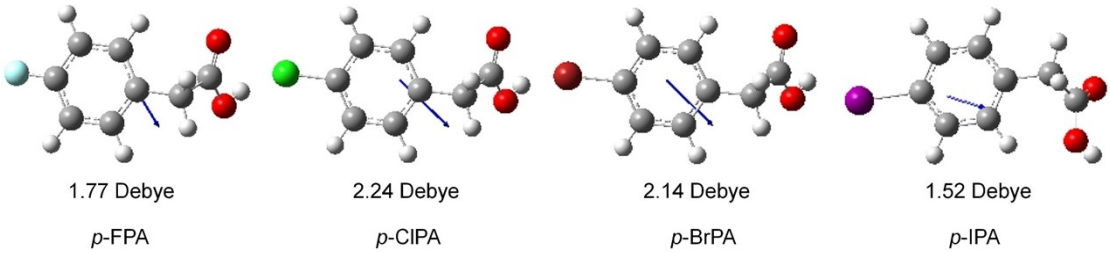

Fig. S2. Dipole moments of *p*-FPA, *p*-ClPA, *p*-BrPA, and *p*-IPA.

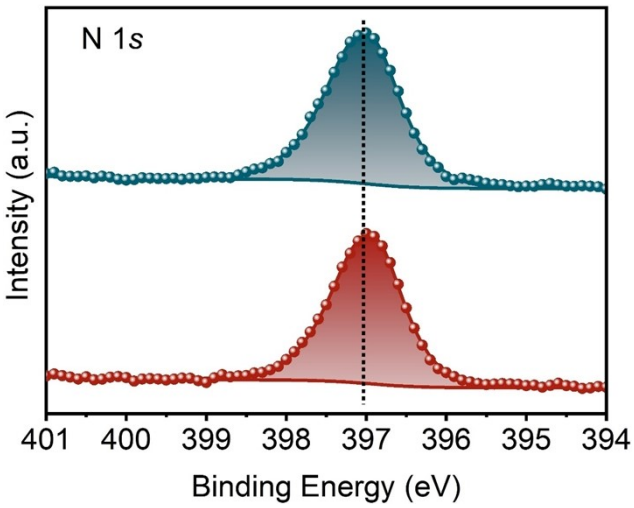

Fig. S3. XPS of N 1*s* for the control and target perovskite films.

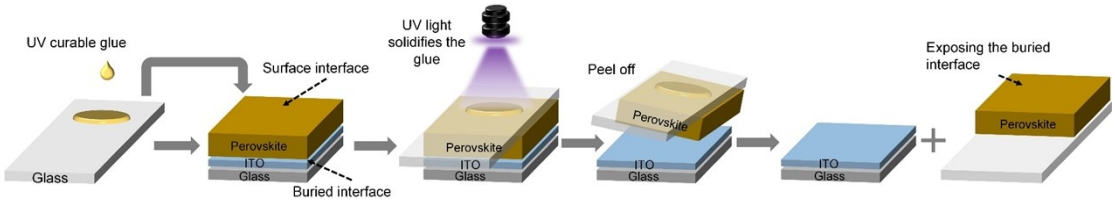

Fig. S4. Schematic diagram of exposing the buried interface of perovskite films.

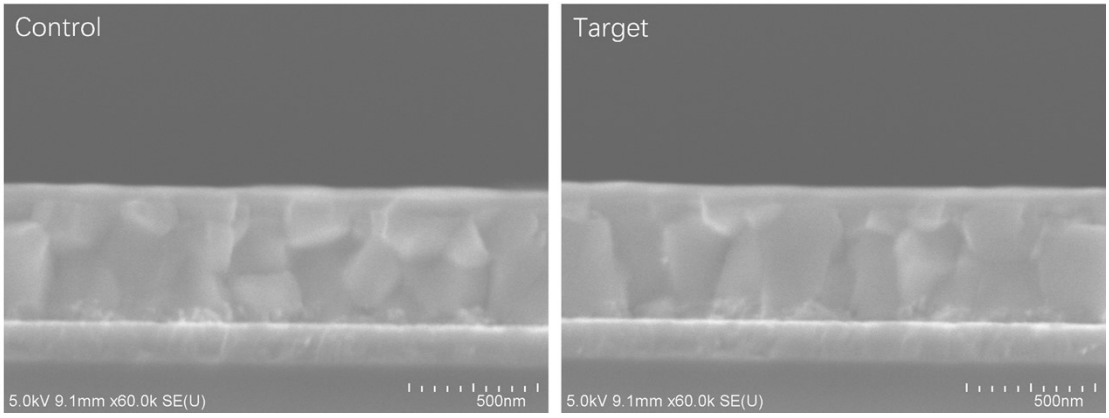

Fig. S5. Cross-sectional SEM images of the control and target devices.

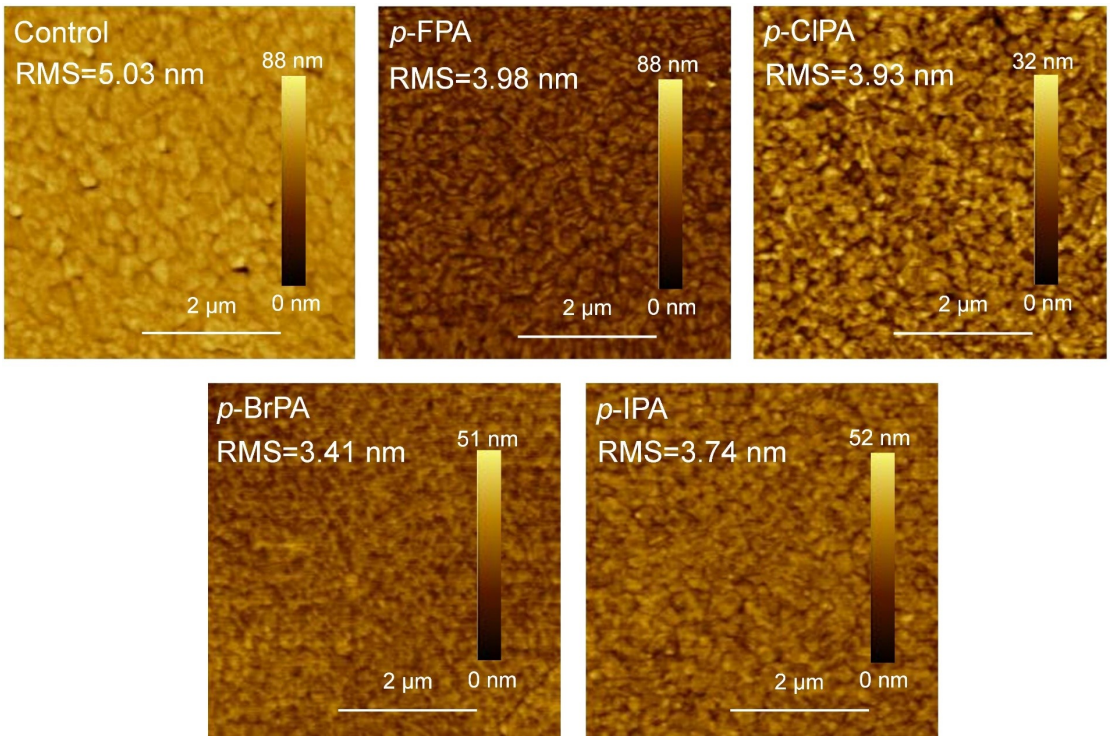

Fig. S6. AFM images of the buried interface of control and *p*-XPA (X=F, Cl, Br, I) modified perovskite films.

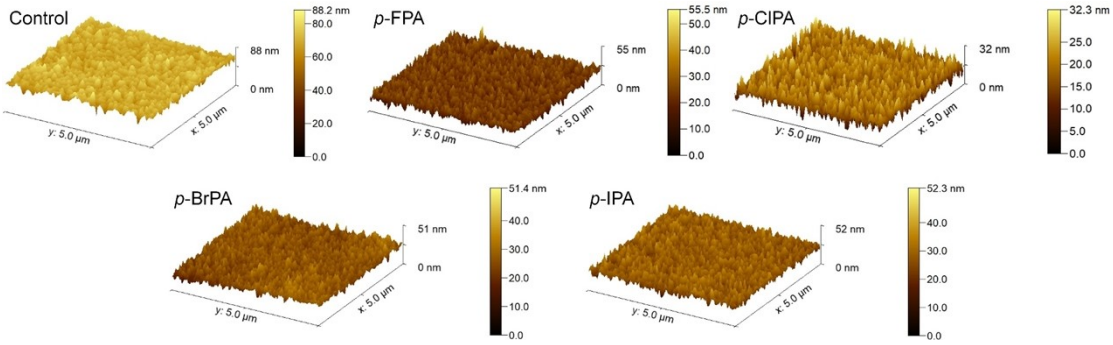

Fig. S7. 3D AFM images of the buried interface of control and *p*-XPA (X=F, Cl, Br, I) modified perovskite films.

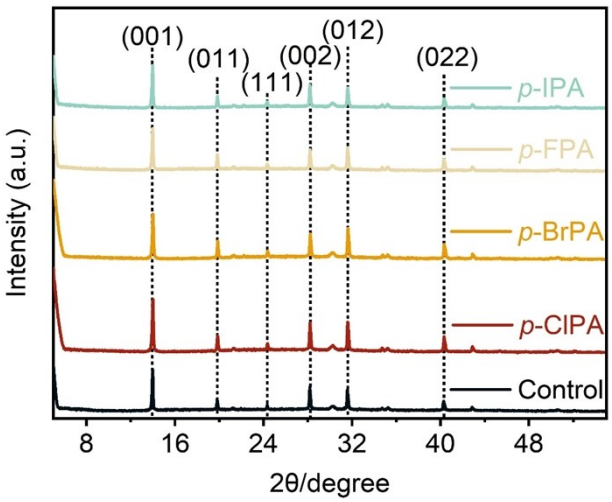

Fig. S8. XRD of control and *p*-XPA (X=F, Cl, Br, I) modified perovskite films.

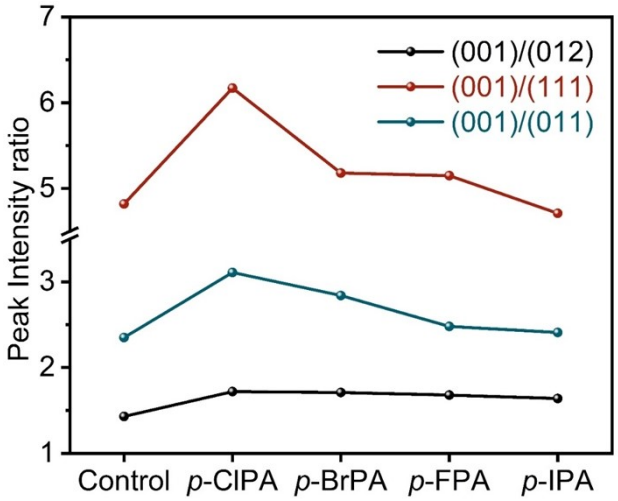

Fig. S9. XRD peak intensity ratio of (001) crystal plane to (012), (111) and (011) calculated by the XRD results of the control and *p*-XPA (X=F, Cl, Br, I) modified perovskite films.

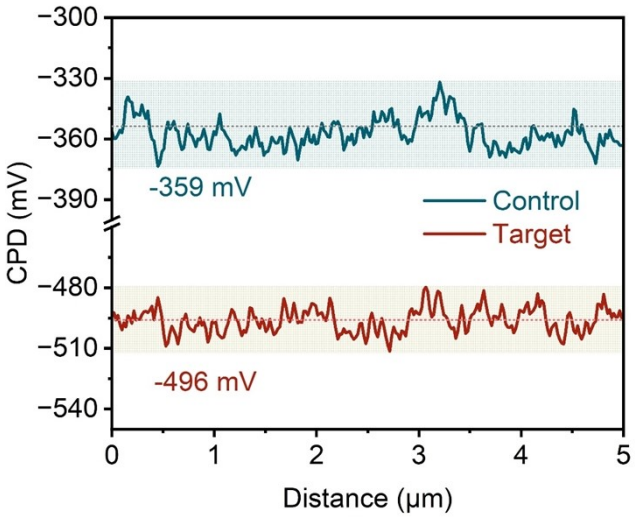

Fig. S10. CPD Statistics of the control and *p*-ClPA modified perovskite films.

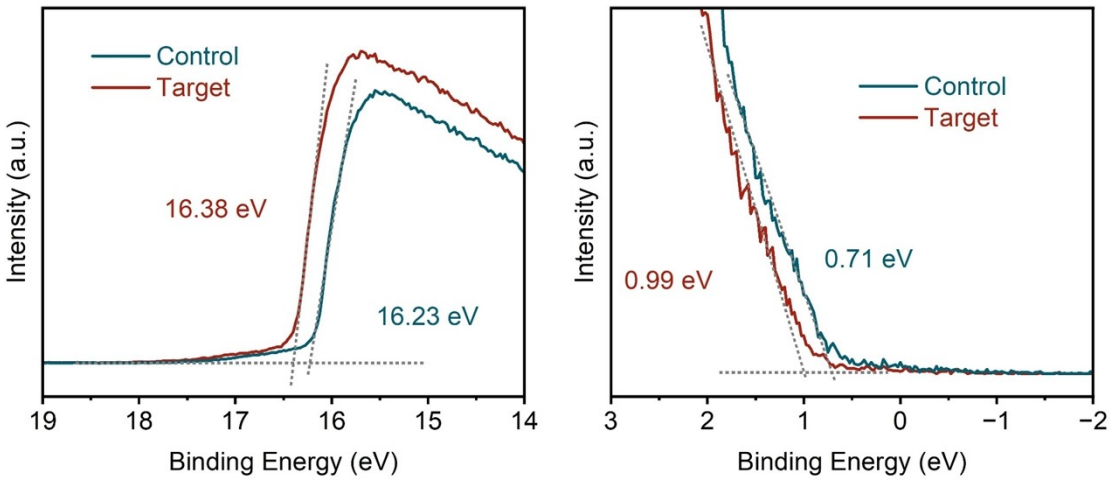

Fig. S11. UPS results of the secondary electron cutoff (left, E_{cutoff}) and onset (right, E_{cutoff}) energy for the control and *p*-ClPA modified perovskite films.

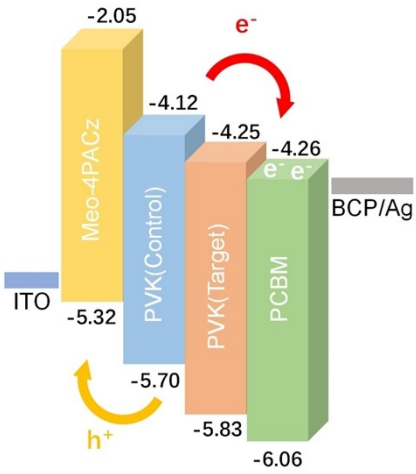

Fig. S12. Energy-level scheme for the control and *p*-ClPA modified perovskite films based on the parameters derived from UPS spectra.

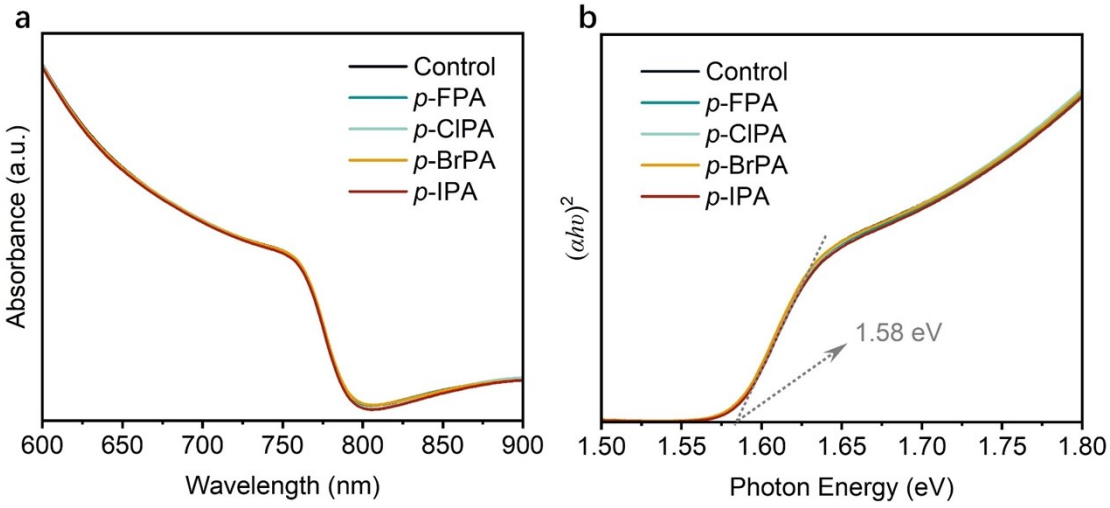

Fig. S13. (a) UV–vis absorption and (b) Tauc plots derived from the UV-vis absorption spectra of the control and *p*-XPA (X=F, Cl, Br, I) modified perovskite films.

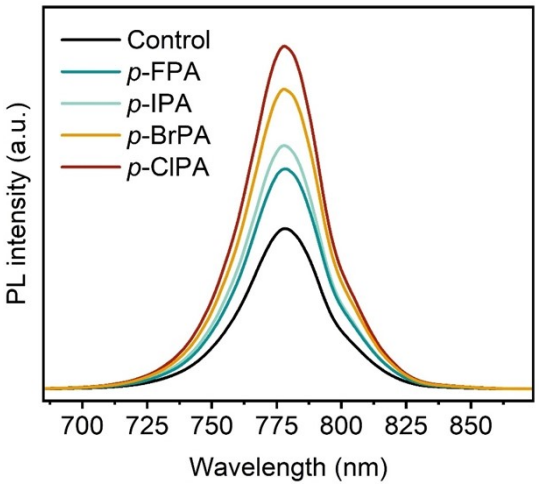

Fig. S14. PL of control and *p*-XPA (X=F, Cl, Br, I) modified perovskite films.

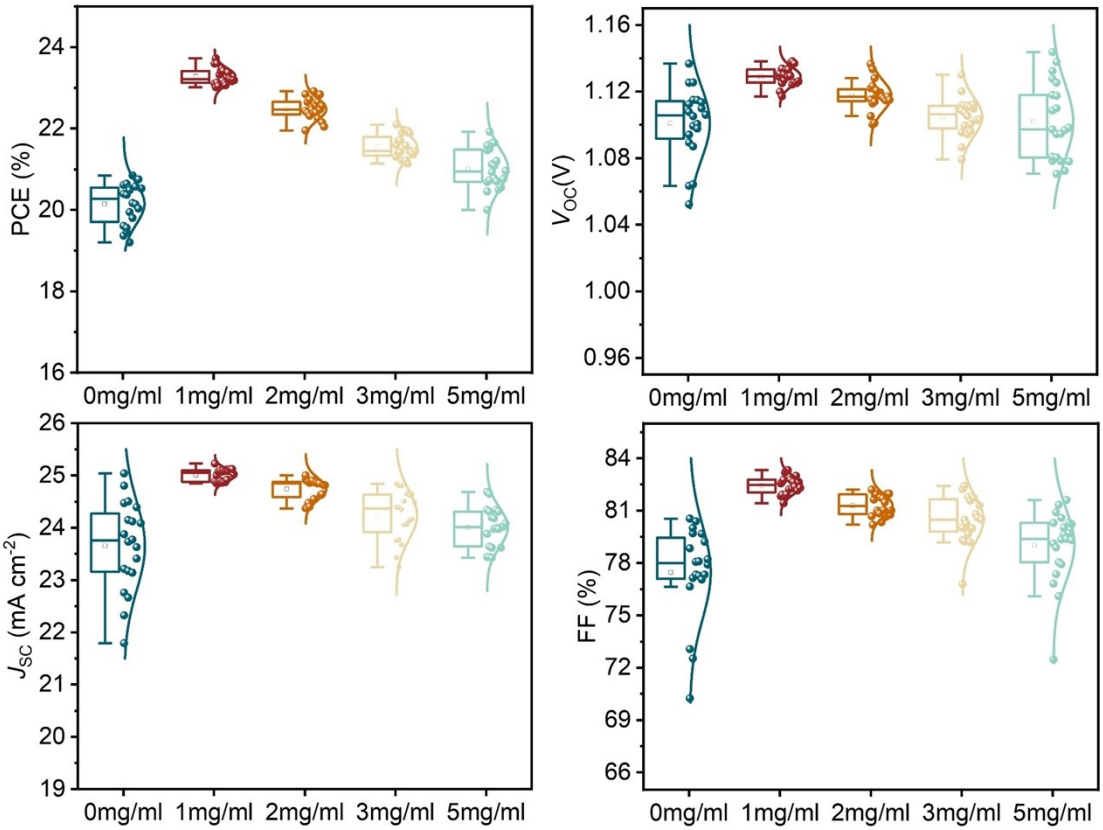

Fig. S15. The impact of *p*-ClPA concentration on device photovoltaic performance.

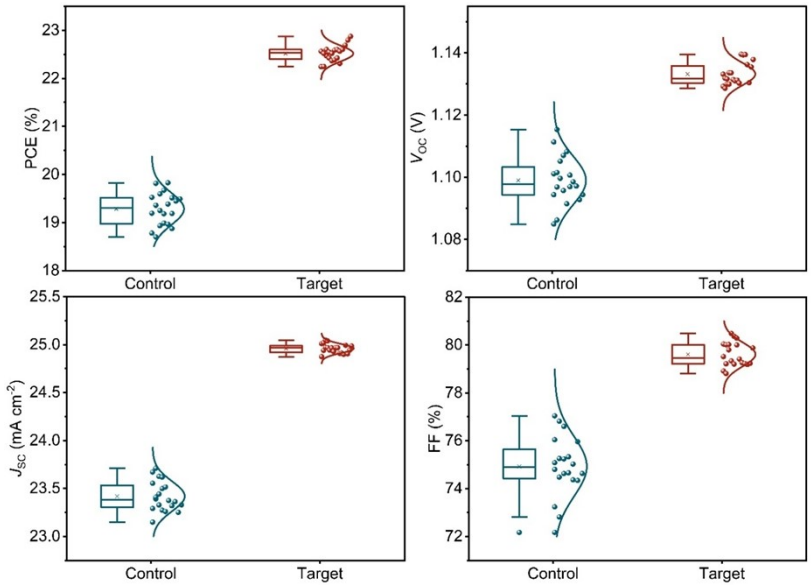

Fig. S16. Performance plots of PCE, V_{OC}, J_{SC} and FF for the control and target devices at an active area of 1.0 cm^2.

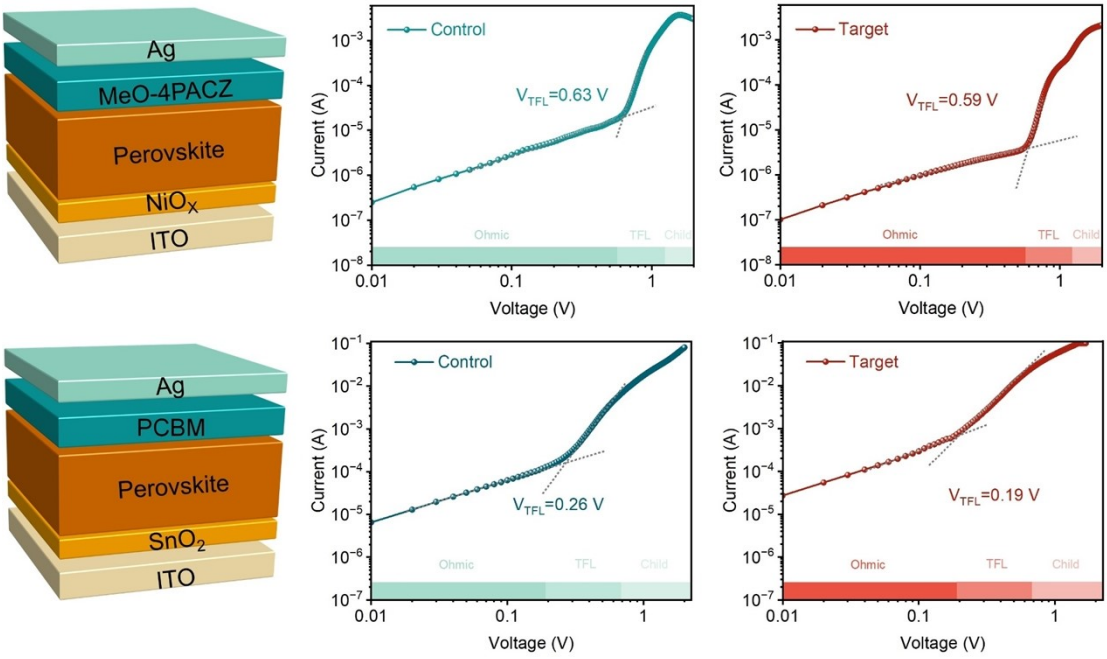

Fig. S17. SCLC measurements of the hole-only and electron-only devices with (target) and without *p*-ClPA (control) modification.

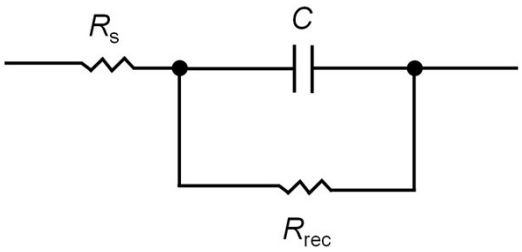

Fig. S18. Equivalent-circuit model from the Nyquist plots of EIS, including the series resistance (R_s), recombination resistance (R_{rec}), and capacitance (C).

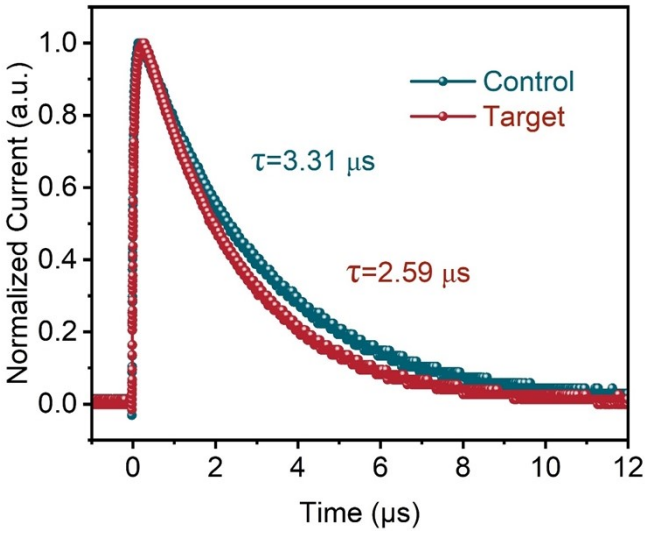

Fig. S19. TPC of the control and *p*-ClPA modified devices.

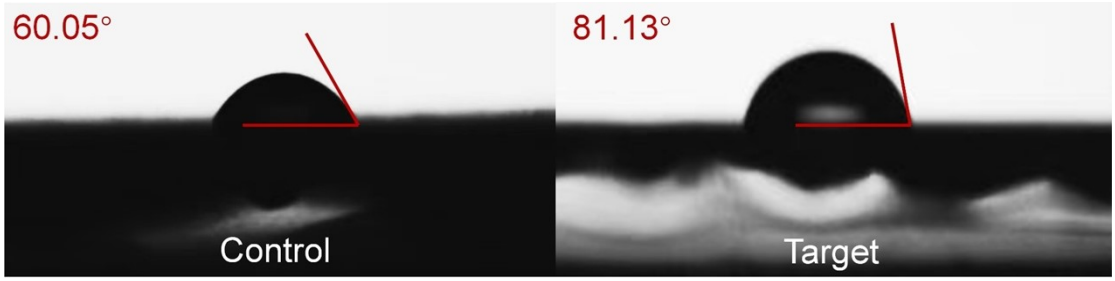

Fig. S20. Water contact angle of the buried interface of control and *p*-ClPA modified perovskite films.

Table S1. Photovoltaic parameters of the control and *p*-XPA (X = F, Cl, Br, I)-treated devices (20 data points for each group, originated from 20 independent devices).

Samples	Champion/average	J_{SC} (mA cm^{-2})	V_{OC} (V)	FF (%)	PCE (%)
Control	Champion	23.63	1.11	79.22	20.85
	Average	23.42±1.63	1.10±0.05	75.39±5.15	20.02±0.83
p-FPA	Champion	25.05	1.10	80.04	22.15
	Average	24.53±0.55	1.09±0.02	77.77±3.80	20.95±1.20
p-ClPA	Champion	25.11	1.14	82.99	23.72
	Average	24.98±0.14	1.13±0.01	82.37±0.95	23.37±0.36
p-BrPA	Champion	24.67	1.13	81.17	22.66
	Average	24.43±0.40	1.11±0.02	80.38±0.15	21.63±1.03
p-IPA	Champion	24.11	1.12	82.21	22.16
	Average	24.27±0.15	1.10±0.02	80.09±2.12	21.12±1.04

Table S2. Electronic parameters of the control and target perovskite films derived from the UPS results.

Sample	E_{cutoff} (eV)	E_{onset} (eV)	VB (eV)	E_g (eV)	CB (eV)
Control	16.23	0.71	−5.70	1.58	−4.12
Target	16.38	0.99	−5.83	1.58	−4.25

Samples	A_1	τ_1 (ns)	A_2	τ_2 (ns)	τ_{ave} (ns)
Control	0.49	111.08	0.37	327.74	260.62
Target	0.16	277.80	0.73	739.97	704.83

Table S3. Summary of TRPL lifetimes for the control and target perovskite films.

Table S4. Parameters of target devices with various *p*-ClPA concentrations.

Concentrations	Champion/average	J_{SC} (mA cm^{-2})	V_{OC} (V)	FF (%)	PCE (%)
0 mg mL^{-1}	Champion	23.63	1.11	79.22	20.85
	Average	23.42±1.63	1.10±0.05	75.39±5.15	20.02±0.83
1 mg mL^{-1}	Champion	25.11	1.14	82.99	23.72
	Average	24.98±0.14	1.13±0.01	82.37±0.95	23.37±0.36
2 mg mL^{-1}	Champion	24.86	1.13	81.71	22.91
	Average	24.69±0.31	1.12±0.02	81.20±1.01	22.43±0.48
3 mg mL^{-1}	Champion	24.35	1.11	81.77	22.10
	Average	24.05±0.80	1.11±0.03	79.61±2.82	21.62±0.48
5 mg mL^{-1}	Champion	23.99	1.14	80.31	21.92
	Average	24.06±0.64	1.11±0.04	77.04±4.57	20.96±0.96

Table S5. Fitting parameters of impedance spectroscopy for the control and target devices.

Sample	R_S (Ω)	R_{rec} (Ω)
Control	12.50	990.60
Target	10.46	1299.00